Supporting Information

Ultrafast electrochemical expansion of black phosphorus towards high-yield synthesis of few-layer phosphorene

Jing Li[1,2,‡], Cheng Chen[1,‡], Shule Liu[3], Junpeng Lu[4,5], Wei Peng Goh[6], Hanyan Fang[1], Zhizhan Qiu[1,7], Bingbing Tian[1,2], Zhongxin Chen[1], Chuanhao Yao[1,2], Wei Liu[1], Huan Yan[1,2], Ying Yu[8], Dan Wang[8], Yewu Wang[8], Ming Lin[6], Chenliang Su*[2] & Jiong Lu*[1,5]

[1]Department of Chemistry, National University of Singapore, 3 Science Drive 3, Singapore 117543.

[2] SZU-NUS Collaborative Center and International Collaborative Laboratory of 2D Materials for Optoelectronic Science & Technology, Engineering Technology Research Center for 2D Materials Information Functional Devices and Systems of Guangdong Province, College of Optoelectronic Engineering, Shenzhen University, Shen Zhen, 518060, China.

[3]School of Materials Science and Engineering, Key Laboratory for Polymeric Composite and Functional Materials of Ministry of Education, Sun Yat-Sen University, Guangzhou 510275, P. R. China.

[4]Department of Physics, National University of Singapore, 2 Science Drive 3, Singapore 117542.

[5]Centre for Advanced 2D Materials and Graphene Research Centre, National University of Singapore, Singapore 117546.

[6]Institute of Materials Research and Engineering, Agency for Science, Technology and Research (A*STAR), 2 Fusionopolis Way, Innovis, #08-03, Singapore 138634.

[7]NUS Graduate School for Integrative Sciences and Engineering, National University of Singapore, 28 Medical Drive, Singapore 117456.

[8]Department of Physics & State Key Laboratory of Silicon Materials, Zhejiang University, Hangzhou 310027, P. R. China.

[‡]These authors contributed equally to this work.

Table of contents:

1. Experimental methods.

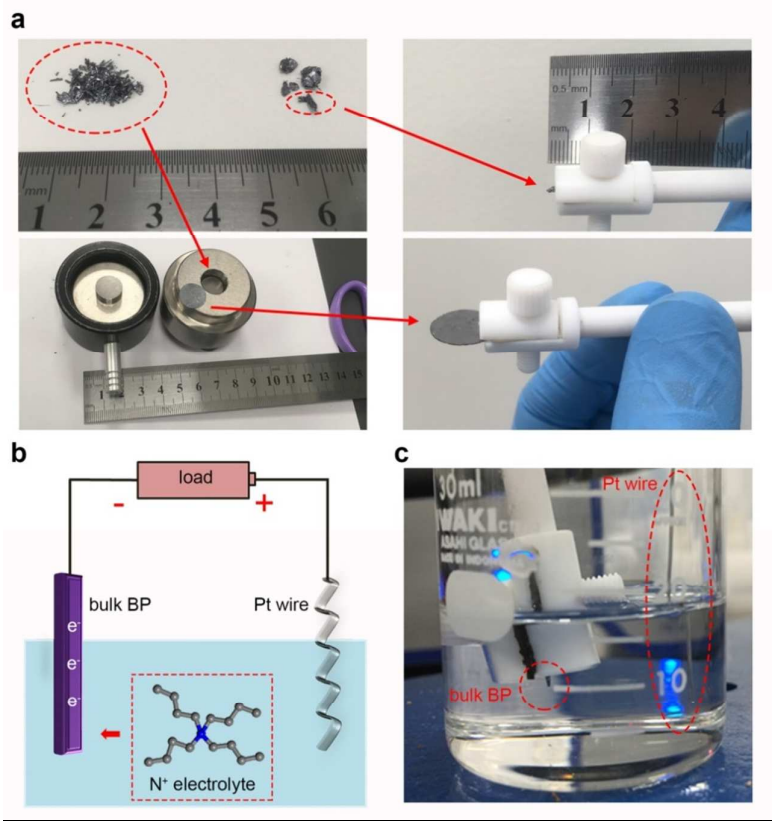

Figure S1. (a) Photographs of as-received bulk BP samples, BP flakes and disks mounted to the Pt clamp electrode. (b) Schematic illustration and (c) photograph of the electrochemical exfoliation of bulk BP in ambient conditions.

Commercial bulk BP samples often exhibit irregular shape with different sizes and thicknesses. The millimeter sized BP (several milligrams) can be directly mounted onto the Pt clamp electrode using the Teflon screw as shown in Figure S1a. As for the

large-scale exfoliation of bulk BP, the BP powder will be compressed into the round disk with a diameter of ~1 cm using a die-set (Figure S1a) for the subsequent electrochemical exfoliation in ambient conditions.

2. Cyclic voltammetry measurement and *in-situ* visualization of electrochemical charging of bulk BP during CV measurements.

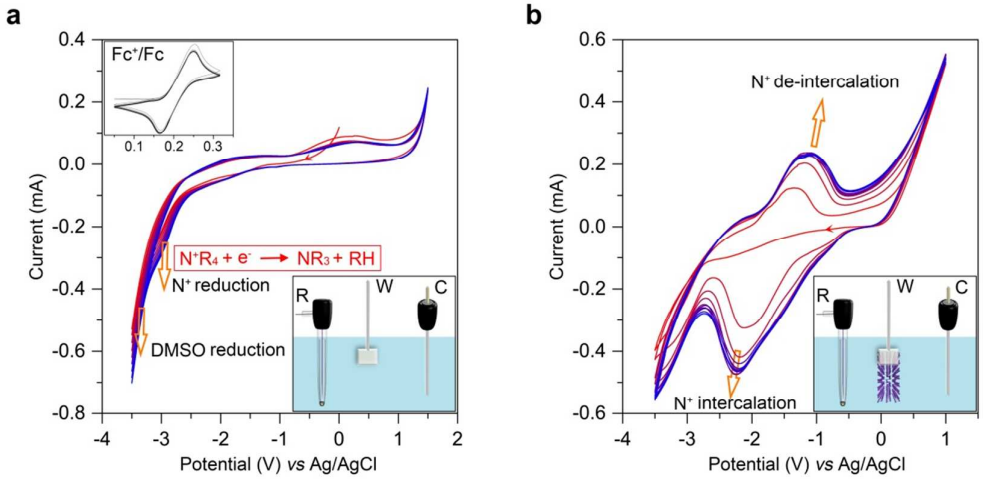

Figure S2. Three-electrode cyclic voltammetry curves of Pt clamp (a) without and (b) with bulk BP (~5 mg, 1 mm×1 mm×5 mm) as working electrode (labeled as **W** in the lower inset) in 0.01 M TBAB solution of DMSO. The scan rate: 0.05 *V*/s, reference electrode (**R** in the lower inset): Ag/AgCl (0.01 M $AgNO_3$ in DMSO), and counter electrode (**C** in the lower inset): Pt wire. The Ag/AgCl reference potential was calibrated using ferrocene/ferrocenium pseudo reference as shown in the upper inset of panel (a).

Three-electrode CV measurement. To elucidate the structure change of bulk BP as a function of voltage applied on it, we employed the three-electrode cell characterization of bulk BP compared with the blank Pt clamp electrode in the organic electrolyte of tetrabutylammonium tetrafluoroborate (TBAB) and DMSO as shown in Figure S2. We used ferrocene/ferrocenium pseudo reference electrode for the potential calibration (the upper inset of Figure S2a). The reference potential of Ag/AgCl electrode in DMSO is determined to be ~0.3 *V versus* normal hydrogen

electrode.[1] Figure S2a shows the 10 consecutive CV scans of blank Pt clamp as working electrode in the electrolyte containing 0.01 M TBAB/DMSO. The rapid increase of cathodic current for the voltage lower than -3 *V* can be attributed to the cathodic decomposition of TBAB (and DMSO) into tributylamine and butane (and dimethyl sulfite as in Figure S3) as illustrated in Figure S2a.[2] Furthermore, we carried out CV measurements of bulk BP mounted on Pt clamp under the same electrochemical condition (as shown in Figure S2b) compared with that of bare Pt working electrode. It is observed that a gradual increase of cathodic current occurs for the voltage lower than -2.3 *V* due to the intercalation of TBA^+ ions into the BP host[3, 4]. In addition, the anodic peak ~-1.5 *V* can be ascribed to the de-intercalation of TBA^+ ions. Interestingly, the cathodic and anodic peak positions of BP electrode exhibit a continuous shift towards more negative and positive potential direction respectively as the number of CV scan increases. Furthermore, the redox current also continues to increase as a function of the number of CV scan, suggesting that the surface area of BP electrode has been enlarged due to the electrochemical expansion of BP in the process of CV measurements.

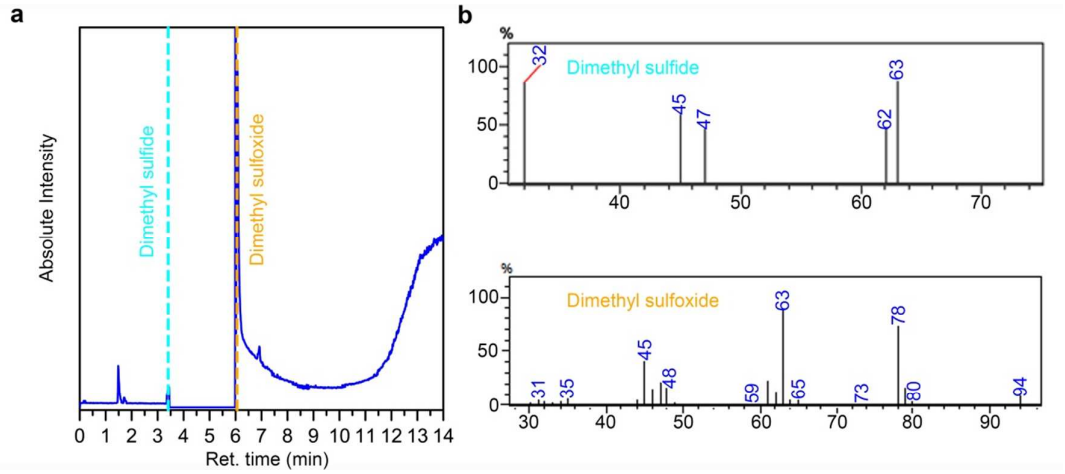

Figure S3. GC-MS characterization of TBAB/DMSO electrolyte after the electrochemical exfoliation of bulk BP.

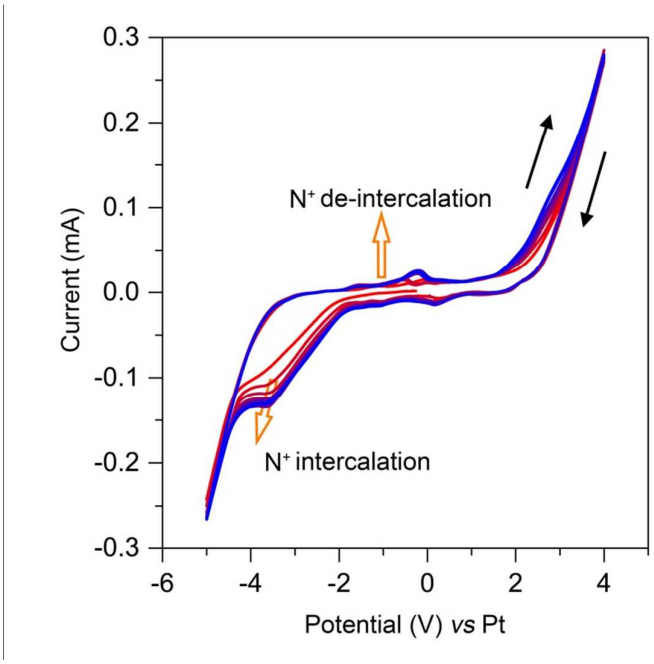

Figure S4. Cyclic voltammetry curves (at a scan rate of 0.1 V/s) of bulk BP (~5 mg, 1 mm×1 mm×5 mm) in 0.001 M TBAB in DMSO solution (Voltage *vs*. Pt wire, a two-electrode cell).

In-situ **visualization of electrochemical charging of bulk BP during CV measurements.** For the combination with optical microscope and facial exfoliation of bulk BP, a two-electrode cell CV measurement was carried out. Figure S4 shows the 10 consecutive scans of CV of bulk BP (Pt wire was used as the counter electrode) in the electrolyte containing 0.001 M (a relatively lower concentration used here to slow down the expansion process for the ease of observation) TBAB in DMSO solvent. In the CV measurement, the cathodic current increases gradually as the potential is swept from -0.3 *V* (open circuit voltage) to -3.5 V, which can be attributed to the intercalation of TBA cations into the interlayer space of BP. As the voltage is further decreased beyond -4 *V,* the reduction current increases rapidly due to the cathodic decomposition of DMSO[5] and TAA ions[6] produces the gaseous species such as dimethyl sulfite (Figure S3) and alkane[6], resulting in a dramatic volume expansion

and efficient exfoliation of BP, leading to an ultrafast expansion of bulk BP. During the reverse scan, a new peak emerges around 0 *V* accompanying with the observation of noticeable shrinkage of BP electrode, presumably due to de-intercalation of solvated TBA cations. In summary, the electrochemical process in two-electrode system is consistent with that of three-electrode system except for the relative potential difference (about 1.2 *V*) between reference electrode of Pt and Ag/AgCl.

3. **Probe the role of electrolyte solvent on the electrochemical expansion of bulk BP.**

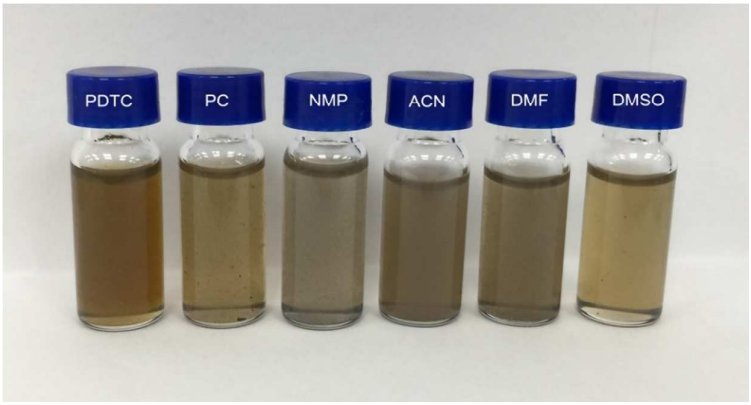

Figure S5. Electrochemical exfoliation of BP using 0.01 M TBA salts dissolved in a series of polar aprotic solvents including Pyrrolidine dithiocarbamate (PDTC), propylene carbonate (PC), N-Methyl pyrrolidone (NMP), acetonitrile (ACN), N,N-Dimethylformamide (DMF) and DMSO.

The role of electrolyte solvent: It is observed that electrochemical intercalation and expansion of BP cannot proceed with polar protic solvents (eg. isopropyl alcohol, water, acetic acid) or nonpolar solvents (eg. toluene, dichloromethane) even when the low charging voltage down to -10 *V* is applied. Such a voltage already exceeds the onset potential of the cathodic decomposition of ammonium ions (~-4 *V vs* Pt)[6] and the organic solvents[5]. Our results reveal that efficient electrochemical expansion of BP occurs when polar aprotic solvents are used to dissolve TAA cations with appropriate sizes (polar aprotic solvents explored include pyrrolidine dithiocarbamate, DMSO, propylene carbonate, N-Methyl pyrrolidone, acetonitrile, and N, N-Dimethylformamide as shown in Figure S5). This finding can be attributed to the following factors: (i) TAA salts can be better dissolved in polar solvents[7]; (ii) Similar surface tension (~40 dyne cm^{-1})[8, 9] of BP and polar aprotic solvents. (iii) The polar

solvent facilitates the formation of solvated TAA cations in the electrolyte[10], which can be driven and inserted into the interlayer gallery of bulk BP at a low cathodic potential ~-3.5 *V vs* Pt, similar to the cathodic charging of graphite; (iv) The electrochemical decomposition of solvated TAA complex into the gaseous species is activated at the cathodic voltage of -4 *V*,[5] creating the gas bubbles for the generation of expansion force to push individual BP layers apart.

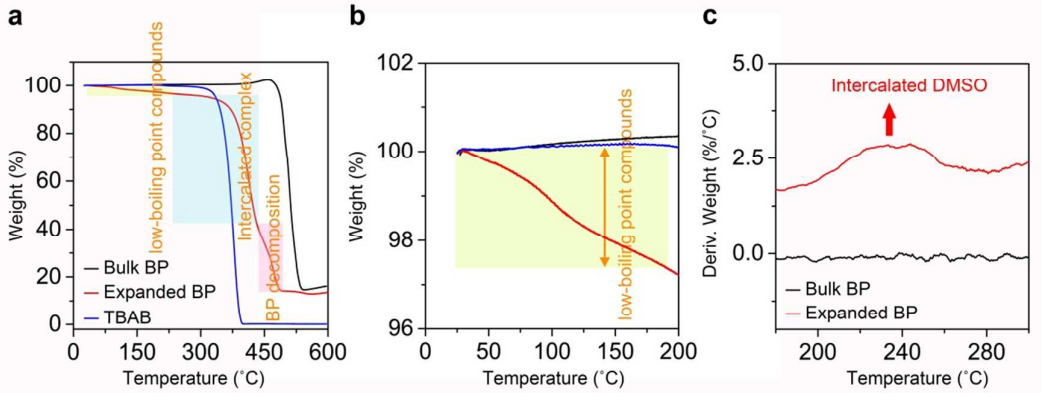

Figure S6. TGA measurement of the expanded BP. (a-b) TGA curves of bulk BP, expanded BP flakes and TBAB powder. (c) The first derivative of TGA curves of bulk BP and exfoliated BP in the temperature range of 180 ˚C to 300 ˚C.

TGA measurement: The expanded BP electrode was filtrated and then dried in nitrogen atmosphere for 24 h to remove the excess solvent adsorbed on the BP surface before TGA measurement. We also performed TGA measurements of the bulk BP and TBAB salt in comparison with that of expanded BP flakes as shown in Figure S6 above. The thermal decomposition of exfoliated BP can be divided into three stages as labelled in Figure S6a: (i) low-boiling point compounds (generated by cathodic decomposition of intercalated complex and trapped in the interlayer space of expanded BP) are released in the temperature window from 30 ˚C to 190 ˚C, resulting

in a 2.5% weight loss. (ii) A 50% weight loss in the temperate range from 190 ˚C to 420 ˚C is mainly contributed from the thermal decomposition of intercalated compounds (solvated TBA cations). (iii) The decomposition of BP between 420 ˚C and 600 ˚C results in a 30 % weight loss. We also observed a small percentage of weight loss in the temperature range of 190 ˚C < T < 260 ˚C attributed to the intercalated DMSO solvents (Figure S6c). The TGA measurements further support the intercalation of solvated TBA cations and their cathodic decomposition into small molecules with low-boiling points.

4. **Characterize the BP thin flakes directly exfoliated from the electrode during the electrochemical charging process.**

A small quantity of large-sized FLBP (> hundreds of micrometers) will be directly detached from BP cathode after charging at -5 *V* for 10 mins. A representative large-sized flake consisting of few layers BP on a SiO_2/Si substrate exhibits a purple color in the optical imaging (Figure S7a). In addition, the thickness of a FLBP flake (Figure S7b-S7d)) is determined to be ~3 nm based on a height profile analysis using AFM (in Figure S7d).

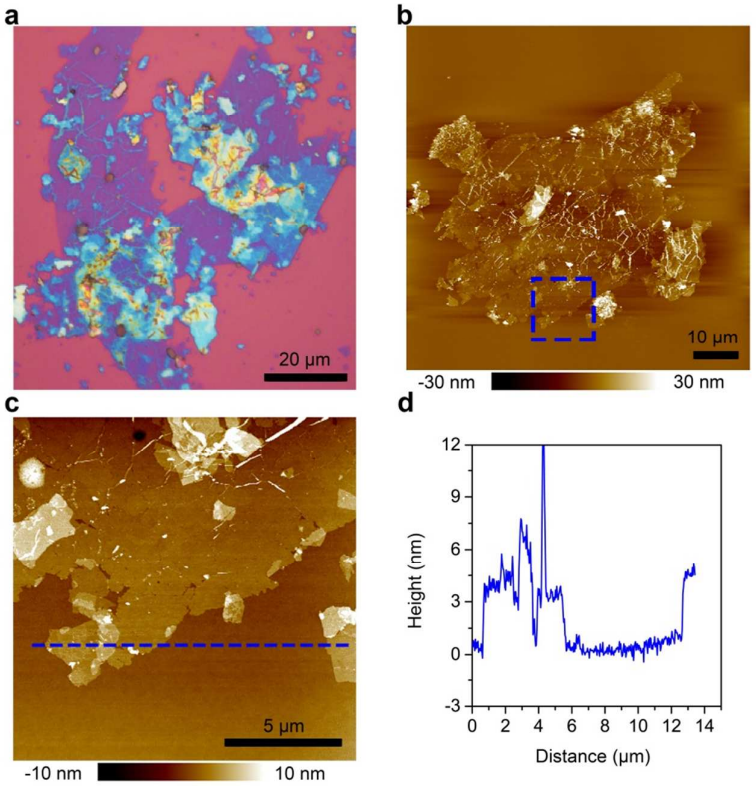

Figure S7. The direct exfoliation of large-sized FLBP flakes from the electrode. (a) Optical and (b-c) AFM imaging of large-sized FLBP thin flakes. Panel (c) is the zoom-in AFM image of the area marked by the dashed rectangle in panel (b). (d) The cross-sectional height profile along the dashed line in panel (c).

5. Investigate the size effect of solvated TAA cations on the exfoliation efficiency of BP.

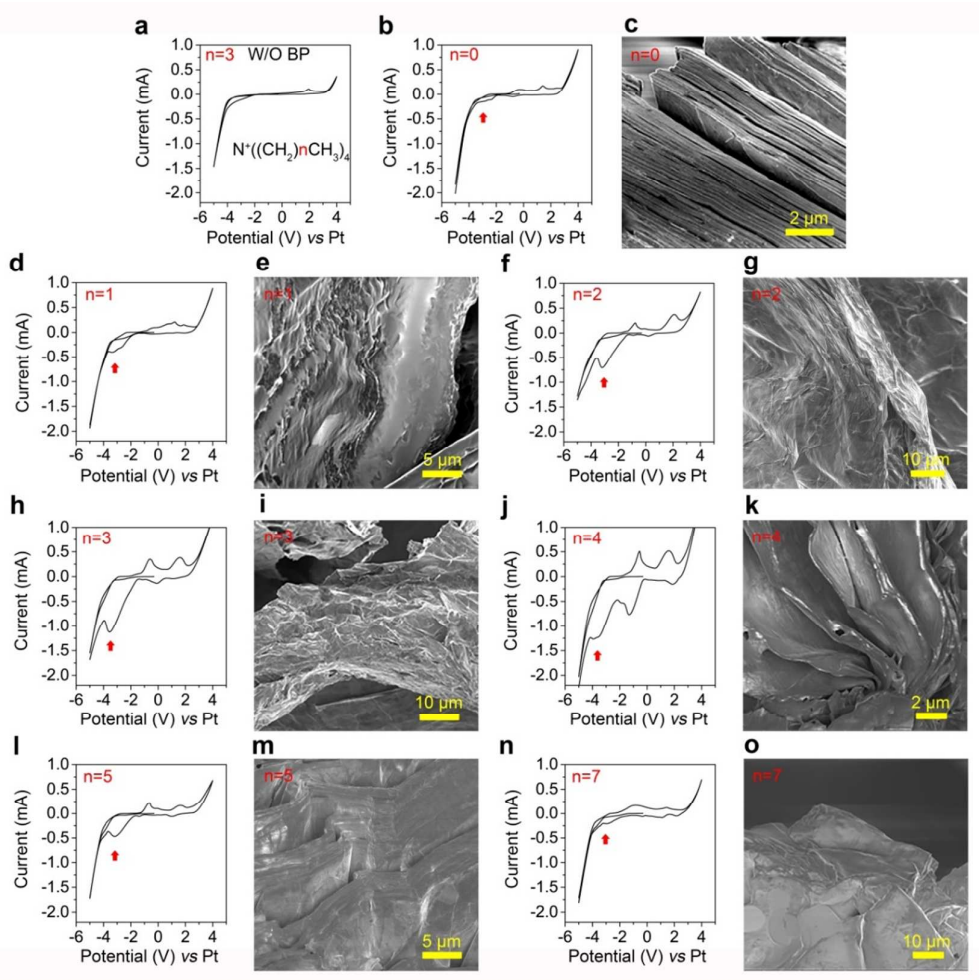

Figure S8. The electrochemical expansion of bulk BP (~5 mg, 1 mm×1 mm×5 mm) using different TAA cations (with the general formula of $N^{+}((CH_2)_nCH_3)_4$). (a) CV curve of blank Pt clamp as working electrode in DMSO electrolyte with 0.01 M TBAB salts. The CV curves (scan rate is 0.1 $V\ s^{-1}$) of bulk BP and the corresponding SEM imaging of the edge of expanded BP in (b-c) tetra-methyl (n=0), (d-e) tetra-ethyl (n=1), (f-g) tetra-propyl (n=2), (h-i) tetra-butyl (n=3), (j-k) tetra-pentyl (n=4), (l-m) tetra-hexyl (n=5) and (n-o) tetra-octyl (n=7) TAA electrolytes (0.01 M).

A series of TAA cations with different substituting groups ranging from tetra-methyl, tetra-ethyl, tetra-propyl, tetra-butyl, tetra-pentyl, tetra-hexyl to tetra-octyl were tested to further optimize the expansion and exfoliation efficiency of bulk BP (Figure S8 and Figure S9). Bulk BP samples with similar sizes and surface areas (~5 mg) were immersed in 5 ml DMSO electrolyte with 0.01 M TAA ions for the electrochemical charging. We swept the voltage between -5 to 4 *V* at a scan rate of 0.1 V/s (CV measurement) in order to monitor different charging and expansion states of BP. After two cycles of voltage scan, a part of expanded BP sample was taken out for drying before SEM characterization, while the remaining BP was further expanded at -5 *V* for 10 minutes. After that, expanded BP samples were directly sonicated and dispersed in the DMSO electrolyte for the evaluation of the exfoliation efficiency. As shown in Figure S8 above, all the CV curves measured for BP electrodes in different electrolytes exhibit a reduction peak centred around -3.5 *V* (marked by red arrows). Such a peak is absent when blank Pt clamp is used as cathode (Figure S8a). The origin of this peak can be attributed to the cation intercalation of BP. We also observed that the reduction current (around -3.5 *V*) shows a significant increase in the second cycle of CV scan due to an increase in the surface area and capacitance of intercalated BP[11]. The increase of current magnitude in the second cycle of CV can be associated with the intercalation and expansion efficiency of BP in different electrolytes. Moreover, we conducted the cross-sectional SEM imaging of BP after charging to evaluate the degree of its volume expansions as shown in Figure S8. Among all the cations investigated, TBA cation exhibits the greatest exfoliation efficiency in terms of expansion rate (in minutes) and yield of FLBP (> 80%).

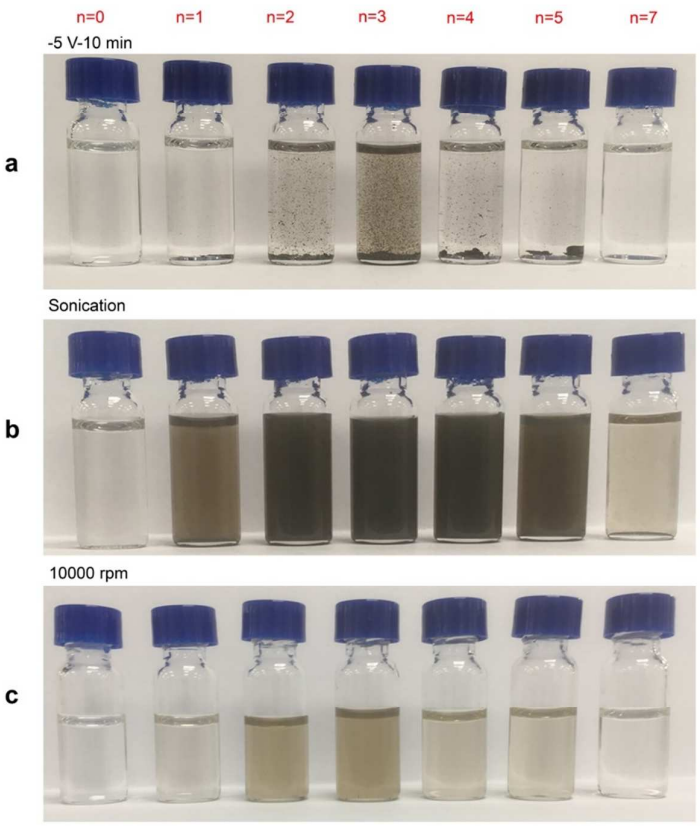

Figure S9. The dispersion of electrochemically-expanded BP flakes synthesized using different TAA salts in DMSO solvent. Note: the BP electrode was charging at -5 *V* for 10 minutes before testing its dispersion in the DMSO solvent (a), sonicating at 100 W for 2 minutes (b) and centrifuging at 10000 rpm for 10 minutes (c).

Typically, the flakes with large thickness or lateral-size are prone to precipitate during centrifugation, which can be used to separate the thin flakes in the solutions from large and thick flakes in the sediment. The colour of solution is associated with the concentration of thin flakes in the dispersion. Among all the cations investigated, the most concentrated FLBP dispersion is obtained using TBA cations (as judged by the darkest brown colour of the dispersion in Figure S9)

6. Molecular dynamic simulation of solvation of TAA cations in DMSO solvents.

Computational Details: Classical molecular dynamics (MD) simulations were performed to calculate the solvated structures of TAA cations using the GROMACS 5.1.4 software[12]. Solvated structures of TAA cations with different alkyl chain length ranging from methyl- to octyl- functional groups in DMSO were studied, and chloride ion was added to the system to maintain the neutrality of the system. For the classical force field parameters of TAA, DMSO and chloride ion, the bonding parameters and Lennard-Jones (LJ) part of the non-bonding parameters were taken directly from the Generalized Amber Force Field (GAFF)[13]. The atomic charges of TAA and DMSO were obtained from the restrained electrostatic potential (RESP)[14] fitting of HF/6-31G* calculation result using the Gaussian 09 software[15], and those charges are given in Table S1. The system contains one TAA cation, one chloride ion and 2811 DMSO molecules to simulate the cation concentration in the range of ~0.01 M. The system was first equilibrated at 1 atm and 300 K in NPT ensemble for 1 ns, and then in NVT ensemble for another 1 ns. After equilibration, a trajectory of 3 ns NVT simulation was collected for solvation structure analysis.

	1	2	3	4	5	6	7	8
N	0.2411	-0.0014	-0.1256	0.2494	0.2165	0.0324	0.1087	0.3229
C1	-0.4106	0.0855	-0.1216	-0.1297	-0.0192	-0.0372	-0.0644	-0.0338
H1	0.2001	0.0608	0.1163	0.0886	0.0576	0.0744	0.0780	0.0496
C2		-0.2458	0.1298	-0.0749	-0.0307	0.0367	-0.0044	0.0024
H2		0.0963	0.0261	0.0572	0.0333	0.0234	0.0334	0.0136
C3			-0.2645	0.0782	-0.0812	-0.0350	0.0235	-0.0122
H3			0.0843	0.0244	0.0576	0.0128	0.0053	0.0146

C4	-0.2612	0.1247	-0.0406	-0.0239	0.0366
H4	0.0782	-0.0039	0.0145	0.0034	-0.0019
C5		-0.2261	0.1455	-0.0119	-0.0108
H5		0.0638	-0.0122	0.0076	0.0000
C6			-0.2477	0.1271	-0.0215
H6			0.0648	-0.0101	0.0061
C7				-0.2464	0.1395
H7				0.0627	-0.0162
C8					-0.2384
H8					0.0586

Table S1. The atomic charges of TAAs with alkyl chain length ranging from one to eight carbon atoms, in unit of elementary charge *e*.

Computational results: Figure S10 shows the radial distribution functions (RDFs) between the nitrogen atom in TAA and the sulfur atom in DMSO. In this case, the RDFs represent the solvent density as a function of the distance from the TAA molecule center. According to the first peak of RDFs in Figure S10a, DMSO has the largest density in the first solvation shell around TMA. As the number of substitutional carbon atoms increases in TAA, the maximum radial density of DMSO in the first solvation shell decreases and then reaches a stable value gradually. This suggests that as the alkyl chain length increases, there is less space accessible to the DMSO molecules in the first solvation shell due to repulsions from the alkyl chains. Moreover, by integrating the RDFs, we could obtain the coordination number (CN), which shows the number of solvent molecules within a certain distance from the TAA molecule center, as is shown in Figure S10b. Therefore, the number of solvent

molecules in the first solvation shell can be obtained from the value of coordination number at the boundary of the first solvation shell, which is the first minimum on the RDF curve.

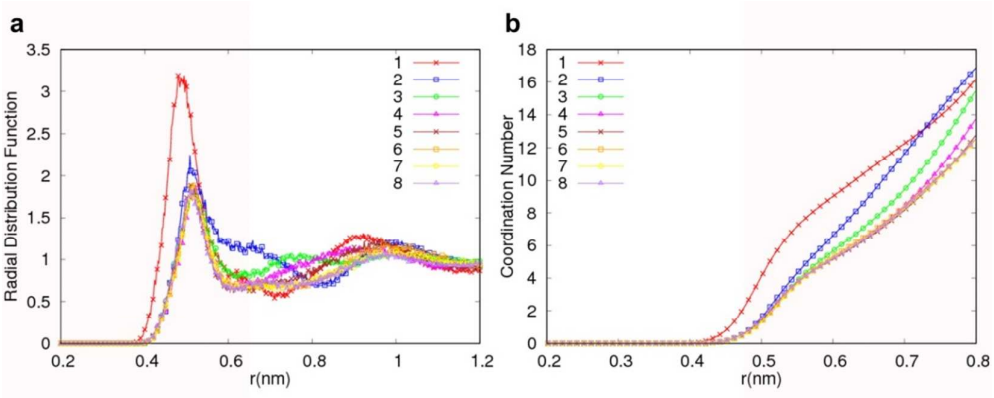

Figure S10. (a) Radial distribution functions between the nitrogen atom in TAA and the sulfur atom in DMSO. (b) Coordination number obtained by integrating the radial distribution function.

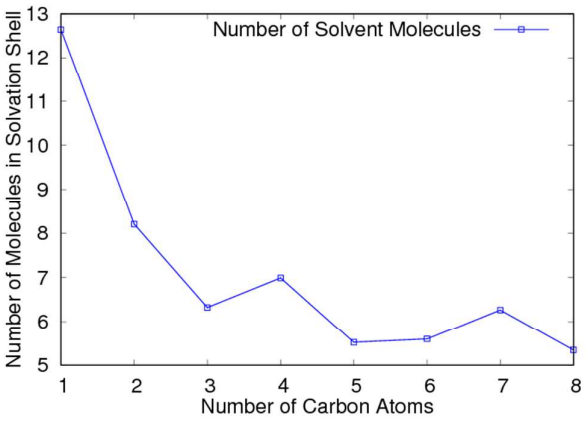

Figure S11. The number of DMSO molecules in the first solvation shell as a function of alkyl chain length in TAA.

Figure S11 shows the number of solvent molecules in the first solvation shell as a function of the alky chain length. In general, as the alkyl chain length increases from methyl to octyl group, the number of DMSO molecules in the first solvation shell decreases, though there is a slight increase from propyl to butyl.

In summary, we found that the size of solvated cations rather than the TAA cation alone plays a key role in determining the efficiency of intercalation of BP, corroborated by experimental results and molecular dynamic simulations.

(i) First, we would like to emphasize that the structural disruption of BP layers observed in this study are mainly due to the cathodic decomposition of intercalated species (rather than the physical transformation of the conformation of TAA ions), which generates massive gas bubbles and creates a large force to push the individual layers apart. TAA ions with different substituted alkyl group show similar

electrochemical properties (refer to CV curves in Figure S12 below). According to the previous reports,[16] the electrochemical decomposition of tetraalkyl ammonium (TAA, general formula is $N^{+}R_4$) occurs between the C-N bond (rather than C-C bond) with the formation of trialkyl ammonium (NR_3) and alkane (RH). Hence, the total amount of gas species generated from the decomposition of TAA ions with different alkyl group will be mainly dependent on the total amount of intercalated TAA compound in the interlayer space of host BP. The intercalation barrier of BP using the smaller tetramethylammonium (TMA) ion is expected to be lower compared to larger sized TAA ions. If this is the case, a larger amount of TMA ions are expected to intercalate into the interlayer space of BP. Hence, the cathodic decomposition of these intercalated compounds at -5 *V* would produce sufficient gaseous bubbles to expand and push layers apart. However, the smallest TMA cations are found to exhibit a negligible exfoliation effect presumably due to insufficient amount of intercalated species. This means that the electrochemical intercalation and decomposition of TAA cations (unsolvated) cannot fully explain the expansion mechanism of BP.

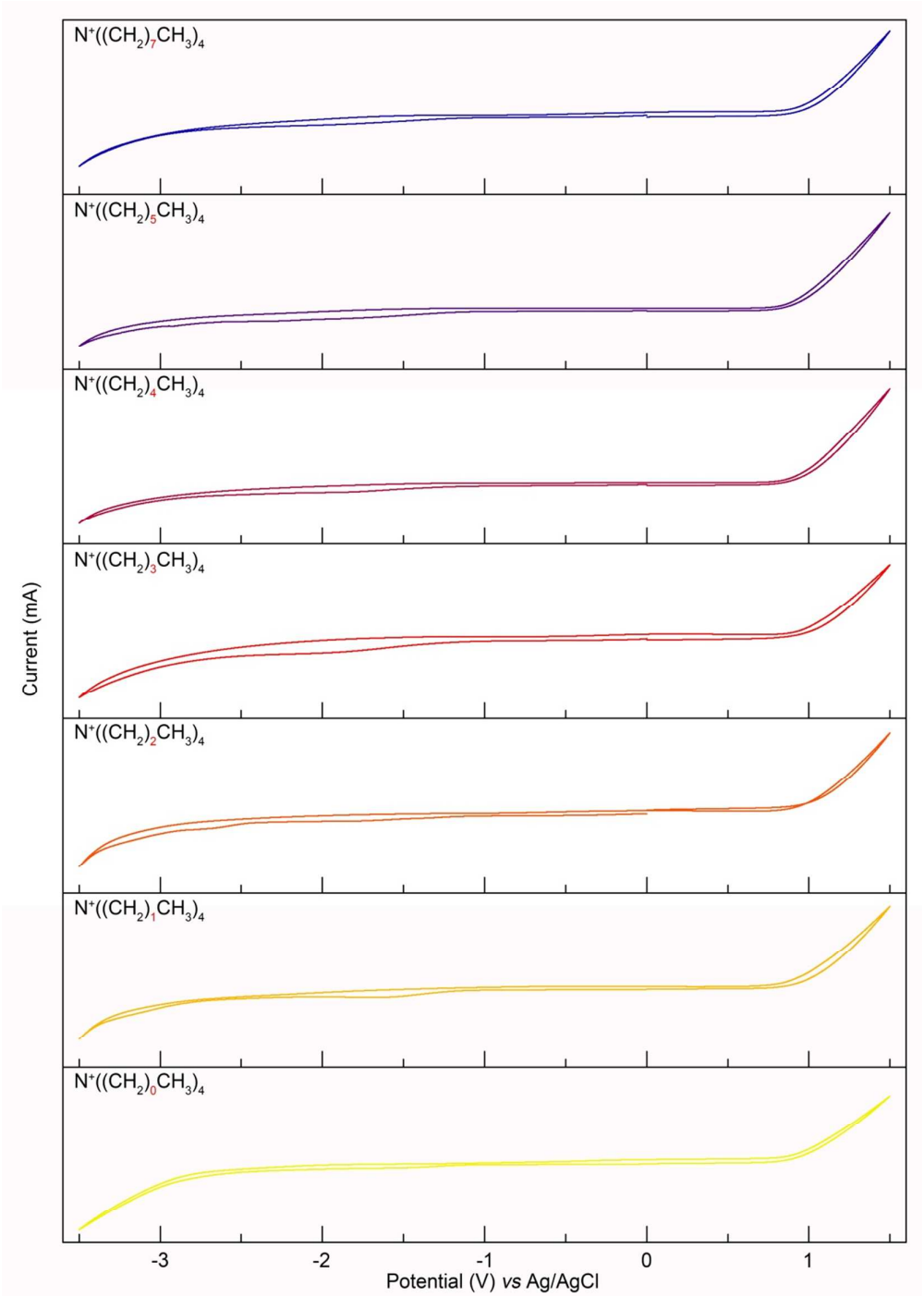

Figure S12. Three-electrode cyclic voltammetry curves of Pt working electrode in a series of 0.01 M TAA ions in DMSO. The scan rate was of 0.1 *V*/s, reference electrode was Ag/AgCl (0.01 M $AgNO_3$ in DMSO), and counter electrode was Pt wire. TAA ions (n=0 to 7) used in this work are electrochemically decomposed at similar reduction potential around -3 *V vs* Ag/AgCl. With the cathodic voltage of -3.5

V vs Ag/AgCl (~ -5 *V vs* Pt in two-electrode cell), both the TAA ions and DMSO solvent can be electrochemically decomposed.

(ii) Secondly, it is observed that TBA (in DMSO) exhibited the greatest exfoliation efficiency in terms of expansion rate and yield of FLBP among all the cations investigated. Based on this observation, we would expect that TBA ions should work equally well for the intercalation and expansion of BP in any solvent that is capable of dissolving TBA salt well. However, we found that TBA dispersed in the nonpolar solvent such as toluene and chloroform exhibit a negligible exfoliation effect. The solvation of TBA ions is expected to be significantly reduced in the non-polar solvent.

Therefore, our experimental observation cannot be rationalized without considering the solvation of TAA cations. In addition, the molecular dynamic simulation reveals that the smallest TMA cations are surrounded by the largest number of DMSO molecules to form a large solvation shell, presumably resulting in a high intercalation barrier and thus poor exfoliation efficiency. On the other hand, although the solvated TOA complex contains few solvent molecules, its own bulky structure similarly results in poor intercalation and hence exfoliation efficiency. In contrast, the size of the solvated TBA complex is comparable to the van der Waal radius of TBA cations. The flexibility of the butyl group enables a flattened TBA cation to reduce its vertical dimension to 0.47 nm, resulting in a more efficient intercalation. Hence, our results reveal that the size of solvated cations rather than the TAA cation alone plays a key role in determining the efficiency of intercalation and exfoliation of BP. A judicious choice of solvent and TAA ion can maximize the exfoliation efficiency of BP.

7. Structural characterization of FLBPs using Raman mapping.

AFM images of the exfoliated BP flakes before and after annealing (250 °C for 2 h in H_2/Ar=5/95 forming gas) are shown in Figure S13a-S13b. It is found that some bright dots and line features associated with solvent/organic residual can be removed after thermal annealing, while the overall morphology and thickness of the flakes remain roughly the same after annealing. In addition, all the flakes exhibit the characteristic A_g^1 phonon mode of BP,[17] as revealed in the Raman mapping of the FLBP thin films (Figure S13d) located in the surface region as marked by dashed square in Figure S13c.

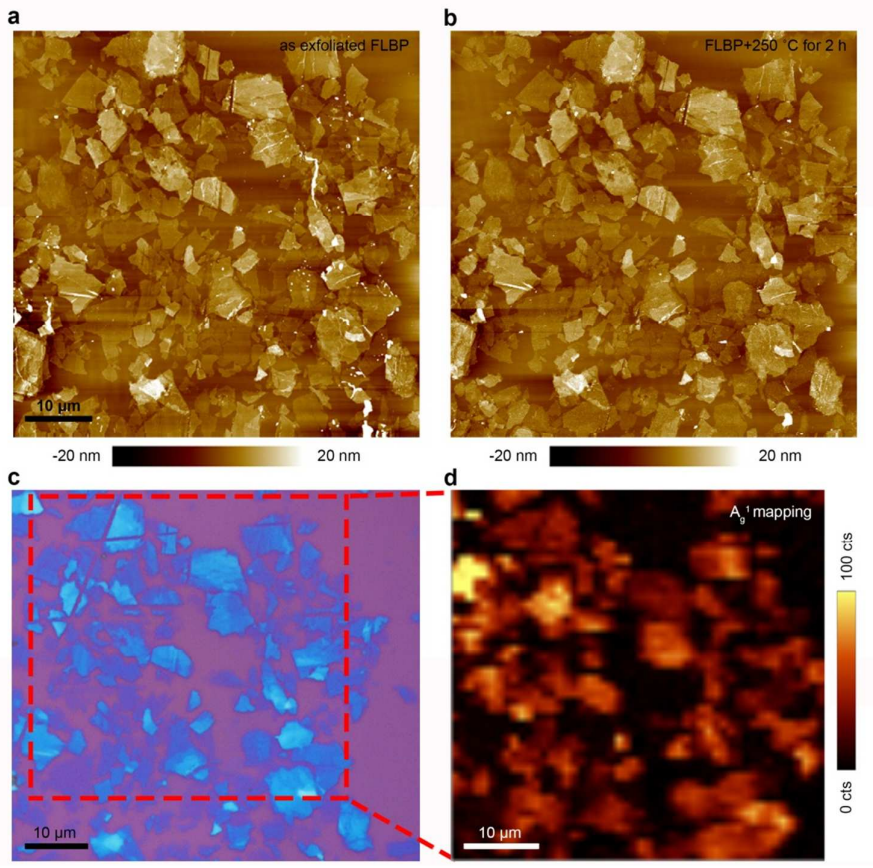

Figure S13. AFM imaging of the exfoliated FLBP (a) before and (b) after annealing at 250 ˚C for 2 h in forming gas (H_2/Ar = 5/95). (c) The optical microscopic image of

the same surface region as shown in (b). (d) Raman mapping (A_g^1) of FLBP thin films located in the region as marked by red dashed rectangle in panel (c).

8. The lateral size and thickness distribution of as-exfoliated FLBP flakes.

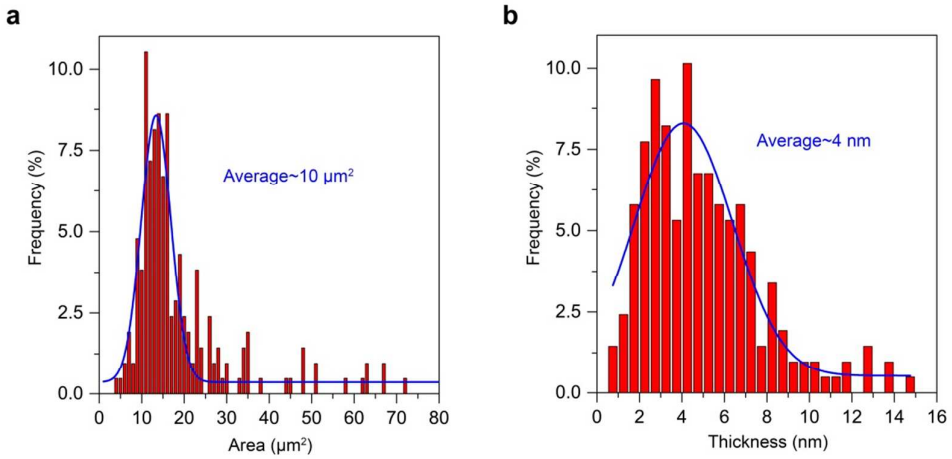

Figure S14. The (a) lateral size (area) and (b) thickness distribution of as-exfoliated FLBP flakes.

9. Optical microscopic images of large-sized BP flakes from monolayer to five layers.

As shown in Figure S15, the large-sized BP thin flakes (tens of micrometers) with different thickness ranging from monolayer to five layers can be obtained *via* the method developed in this work. The thickness-dependent optical contrast reported in the previous work[18] is used to determine the thickness of FLBP flakes imaged in Figure S15.

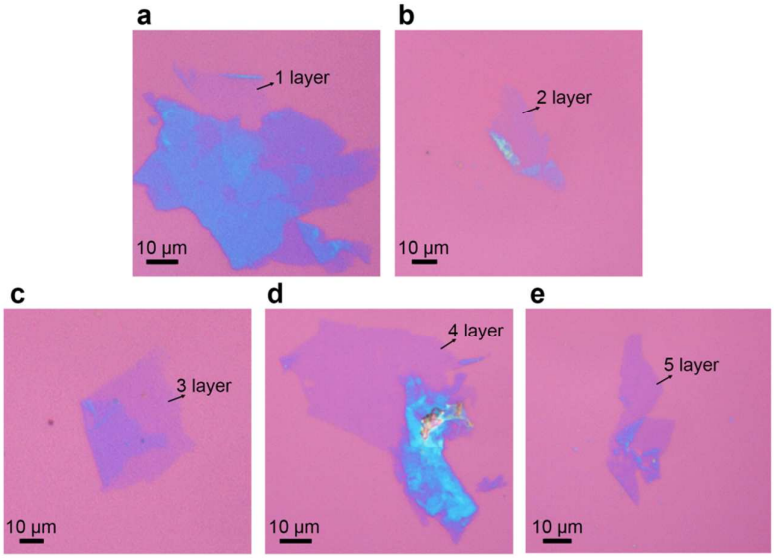

Figure S15. Optical microscopic images of BP flakes with different thickness ranging from monolayer, bi-layer, tri-layer, tetra-layer to penta-layer, respectively.

10. Probe the stability of as-exfoliated FLBP.

We also investigated the air stability of electrochemically-exfoliated FLBP (EEBP) in comparison with that mechanically-exfoliated BP (MEBP) flakes with the similar thickness (~3 nm) and size (~10 μm). Both samples were characterized using tapping mode AFM at room temperature in ambient conditions. The ambient degradation of mechanically exfoliated BP thin flakes occurs shortly after exfoliation (Figure S16f-S16h). In contrast, the EEBP remains stable in air for more than ten hours (Figure S16a-S16b) due to the formation of a solvation shell from the residual solvent molecules which act as a barrier to protect the BP surface from reacting with water or oxygen.[19]

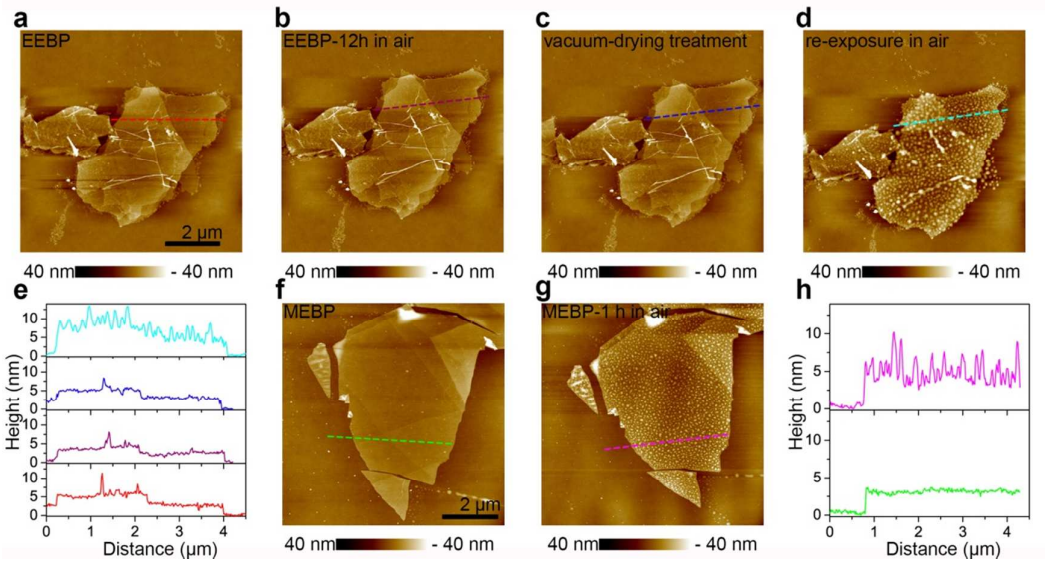

Figure S16. Probe air stability of electrochemically-exfoliated (a-e) and (f-g) mechanically exfoliated FLBP flake with similar thickness and lateral size using AFM.

Figure S16a-S16b show the AFM images of as-electrochemically exfoliated BP (**EEBP)** before (Figure S16a) and after the exposure to air for 12 h in the dark

environment (Figure S16b). Figure S16c-S16d show the AFM images of the **EEBP** after the vacuum drying treatment (10^{-5} Pa for 0.5 h) and its re-exposure to air in dark environment for 1 h. AFM images of as-mechanically exfoliated BP (**MEBP**) before (Figure S16f) and after (Figure S16g) the exposure to air for 1 h in the dark environment. The height profiles along the dashed line marked in each panel are displayed in panel (e) or (f) using the same color scale.

11. FET devices.

FLBP was drop-casted onto a 300 nm SiO_2/Si substrate for the fabrication of back-gated field-effect transistors (FETs). We used a home-made Cu mask (with the channel length of 10-20 μm as in Figure S17) to pattern source and drain electrodes consisting of Cr/Au films with a thickness of 3 nm/50 nm. FET measurements were conducted in ambient conditions using a Keithly 4200 semiconductor parameter analyzer. The field-effect mobility was extracted from the slope ($\Delta I_d/\Delta V_g$) of the linear regime of the transfer curves using the equation[20]:

$$\mu = (L/WC_iV_d) \times (\Delta I_d/\Delta V_g)$$

In which L, W and C_i is the channel length, channel width and capacitance of 300 nm SiO_2, respectively. We have tested ~40 FET devices based on individual FLBP flakes to assess their charge transport properties.

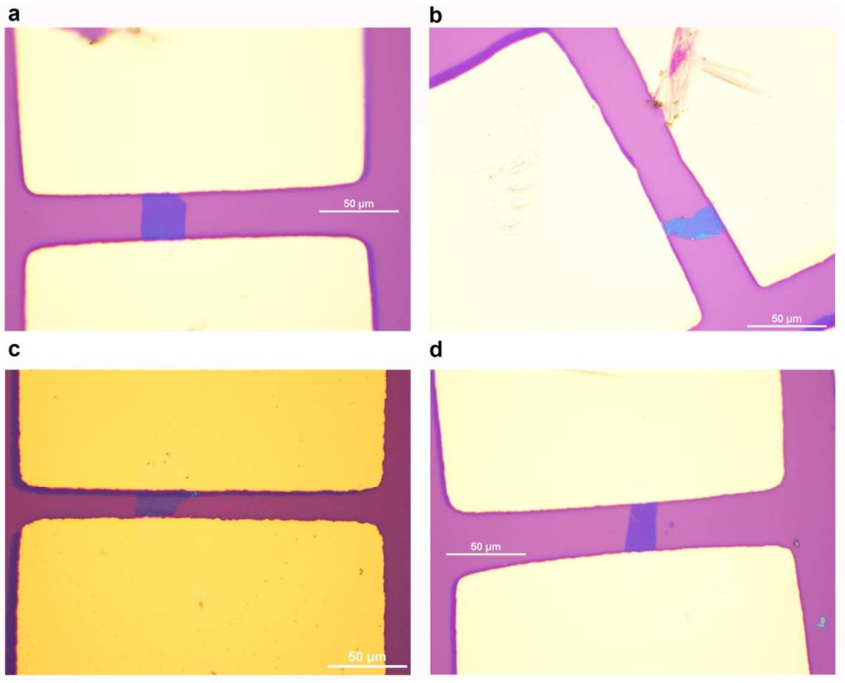

Figure S17. The optical microscopic images of typical FLBP FET devices measured in this work.

BP thickness	Exfoliation methods	Hole mobility	Ion/Ioff	Temperature (K)	Channel length	Ref
18.7 nm	Mechanical exfoliation	170.5	300	300	3	ACS Nano 2014, 8, 10035-10042
15 nm	Mechanical exfoliation	600	10^5	300	1	Nat. Commun. 2014, 5, 4458
5 nm		205	10^5	120		
2 nm		50	5×10^5	120	1	
10nm	Mechanical exfoliation	300	10^3	300	1.5	Appl Phys Lett, 2014, 104(10): 103106
			10^5	<200		
8.9 nm	Mechanical exfoliation	74	10^3	300	0.2	Nano Lett. 2014, 14, 6964-6970
5 nm	Mechanical exfoliation	286	10^4	300	0.2	ACS Nano 2014, 8, 4033-4041
5 nm	Mechanical exfoliation	55	10^5	300	1.6	Nature Nanotech, 2014, 9(5): 372.
Few layers	Exfoliation in NMP	25.9	1.6×10^3	300	0.1-3	ACS Nano 2015, 9, 3596-3604
7.4 nm	Exfoliation in DMF	0.58	10^3	300	0.4	Adv. Mater. 2015, 27, 1887-1892
10 nm	Exfoliation in water	242	5×10^3	300	2.7	Adv. Mater. 2016, 28, 510-517
(4±2.3) nm	Electrochemical exfoliation	60±12	$(1\pm0.49)\times10^4$	300	10-20	This work

Table S2. A summary of the device characteristics of thin layer BP FET devices.

12. The dispersion of expanded BP in desired solvents.

As shown in Figure S18, the expanded BP can be readily dispersed in an abundance of solvents ranging from non-polar (eg, toluene, chloroform), polar protic (eg, H_2O, acetic acid, isopropanol, dichloromethane) to polar aprotic (eg, ethyl acetate, acetone, acetonitrile) solvents with the mild sonication (100 W for 1-3 minutes).

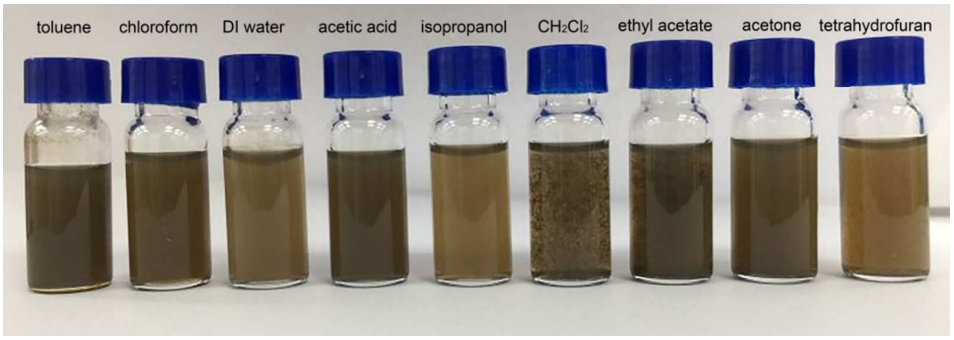

Figure S18. The dispersions of expanded BP in various solvents.

13. The uniformity of FLBP film prepared by inkjet printing.

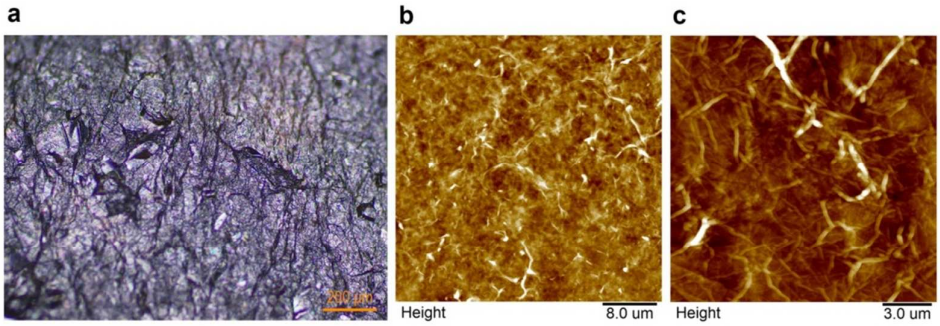

Figure S19. (a) Large-scale optical microscopic image, (b) large-scale AFM image and (c) zoom-in AFM image of inkjet printed BP thin films on the PET substrate.

Reference

(1). Tsierkezos, N. G., Cyclic Voltammetric Studies of Ferrocene in Nonaqueous Solvents in the Temperature Range from 248.15 to 298.15 K. *J. Solution Chem.* **2007,** *36,* 289-302.
(2). Aurbach, D., *Nonaqueous electrochemistry*. CRC Press: 1999.
(3). Besenhard, J. O.; Fritz, H. P., Cathodic reduction of graphite in organic solutions of alkali and NR4+ salts. *Journal of Electroanalytical Chemistry and Interfacial Electrochemistry* **1974,** *53,* 329-333.
(4). Ue, M.; Ida, K.; Mori, S., Electrochemical Properties of Organic Liquid Electrolytes Based on Quaternary Onium Salts for Electrical Double‐Layer Capacitors. *J. Electrochem. Soc.* **1994,** *141,* 2989-2996.
(5). Luca, O. R.; Gustafson, J. L.; Maddox, S. M.; Fenwick, A. Q.; Smith, D. C., Catalysis by electrons and holes: formal potential scales and preparative organic electrochemistry. *Org Chem Front.* **2015,** *2,* 823-848.
(6). Zhong, Y. L.; Swager, T. M., Enhanced Electrochemical Expansion of Graphite for in Situ Electrochemical Functionalization. *J. Am. Chem. Soc.* **2012,** *134,* 17896-17899.
(7). Ralston, A. W.; Reck, R. A.; Harwood, H. J.; DuBrow, P. L., The Solubilities of Long-Chain Dialkyldimethyl-Ammonium Chlorides In Organic Solvents. *J. Org. Chem.* **1948,** *13,* 186-190.
(8). Hu, G.; Albrow-Owen, T.; Jin, X.; Ali, A.; Hu, Y.; Howe, R. C. T.; Shehzad, K.; Yang, Z.; Zhu, X.; Woodward, R. I.; Wu, T.-C.; Jussila, H.; Wu, J.-B.; Peng, P.; Tan, P.-H.; Sun, Z.; Kelleher, E. J. R.; Zhang, M.; Xu, Y.; Hasan, T., Black phosphorus ink formulation for inkjet printing of optoelectronics and photonics. *Nat. Commun.* **2017,** *8,* 278.

(9). Hernandez, Y.; Nicolosi, V.; Lotya, M.; Blighe, F. M.; Sun, Z.; De, S.; McGovern, I.; Holland, B.; Byrne, M.; Gun'Ko, Y. K., High-yield production of graphene by liquid-phase exfoliation of graphite. *Nat. Nanotechnol.* **2008,** *3,* 563.
(10). Besenhard, J. O.; Möhwald, H.; Nickl, J. J., Electronic conductivity and structure of DMSO-solvated A+ - and NR4+-graphite intercalation compounds. *Carbon.* **1980,** *18,* 399-405.
(11). Hao, C.; Yang, B.; Wen, F.; Xiang, J.; Li, L.; Wang, W.; Zeng, Z.; Xu, B.; Zhao, Z.; Liu, Z.; Tian, Y., Flexible All-Solid-State Supercapacitors based on Liquid-Exfoliated Black-Phosphorus Nanoflakes. *Adv. Mater.* **2016,** *28,* 3194-3201.
(12). Abraham, M.; Van Der Spoel, D.; Lindahl, E.; Hess, B., The GROMACS development team GROMACS user manual version 5.0. 4. Accessed: 2014.
(13). Wang, J.; Wolf, R. M.; Caldwell, J. W.; Kollman, P. A.; Case, D. A., Development and testing of a general amber force field. *J. Comput. Chem.* **2004,** *25,* 1157-1174.
(14). Bayly, C. I.; Cieplak, P.; Cornell, W.; Kollman, P. A., A well-behaved electrostatic potential based method using charge restraints for deriving atomic charges: the RESP model. *The Journal of Physical Chemistry* **1993,** *97,* 10269-10280.
(15). Frisch, M.; Trucks, G.; Schlegel, H. B.; Scuseria, G.; Robb, M.; Cheeseman, J.; Scalmani, G.; Barone, V.; Mennucci, B.; Petersson, G., Gaussian 09, revision D. 01. Gaussian, Inc., Wallingford CT: 2009.
(16). Finkelstein, M.; Petersen, R. C.; Ross, S. D., The Electrochemical Degradation of Quaternary Ammonium Salts1. *J. Am. Chem. Soc.* **1959,** *81,* 2361-2364.
(17). Favron, A.; Gaufres, E.; Fossard, F.; Phaneuf-Lheureux, A.-L.; Tang, N. Y. W.; Levesque, P. L.; Loiseau, A.; Leonelli, R.; Francoeur, S.; Martel, R., Photooxidation and quantum confinement effects in exfoliated black phosphorus. *Nat. Mater.* **2015,** *14,* 826-832.
(18). Ling, X.; Liang, L.; Huang, S.; Puretzky, A. A.; Geohegan, D. B.; Sumpter, B. G.; Kong, J.; Meunier, V.; Dresselhaus, M. S., Low-Frequency Interlayer Breathing Modes in Few-Layer Black Phosphorus. *Nano Lett.* **2015,** *15,* 4080-4088.
(19). Kang, J.; Wood, J. D.; Wells, S. A.; Lee, J.-H.; Liu, X.; Chen, K.-S.; Hersam, M. C., Solvent Exfoliation of Electronic-Grade, Two-Dimensional Black Phosphorus. *ACS Nano.* **2015,** *9,* 3596-3604.
(20). Li, L.; Yu, Y.; Ye, G. J.; Ge, Q.; Ou, X.; Wu, H.; Feng, D.; Chen, X. H.; Zhang, Y., Black phosphorus field-effect transistors. *Nat. Nanotechnol.* **2014,** *9,* 372-377.